Evaluation of Optical Solder for Fiber-to-Waveguide Coupling in Silicon Photonics

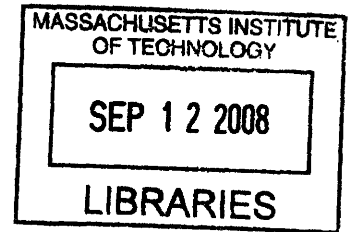
MASSACHUSETTS INSTITUTE OF TECHNOLOGY
SEP 1 2 2008
LIBRARIES

by

Fidelia Tjioe

B.Eng. Materials Engineering
Nanyang Technological University, 2007

SUBMITTED TO THE DEPARTMENT OF MATERIALS SCIENCE AND ENGINEERING IN PARTIAL FULFILLMENT OF THE REQUIREMENTS FOR THE DEGREE OF

MASTER OF ENGINEERING IN MATERIALS SCIENCE AND ENGINEERING

AT THE

MASSACHUSETTS INSTITUTE OF TECHNOLOGY

SEPTEMBER 2008

© 2008 Massachusetts Institute of Technology
All rights reserved

Signature of Author: ....
Department of Materials Science and Engineering
August 8, 2008

Certified by: ....
Lionel C. Kimerling
Thomas Lord Professor of Materials Science and Engineering
Thesis Supervisor

Accepted by: ....
Samuel M. Allen
POSCO Professor of Physical Metallurgy
Chair, Departmental Committee on Graduate Students

ARCHIVES

To my dearest Mom

Evaluation of Optical Solder for Fiber-to-Waveguide Coupling in Silicon Photonics

by

Fidelia Tjioe

Submitted to the Department of Materials Science and Engineering
on August 8, 2008 in Partial Fulfillment of the Requirements for the Degree of
Master of Engineering in Materials Science and Engineering

ABSTRACT

Copper interconnects have shown its limit to meet the bandwidth demand even in the short reach applications due to its increase power consumption, RC delay, EMI, crosstalk and other effects which are aggravated as dimension shrinks. Despite efforts to increase the system performance, e.g. by multicore technology, migration to photonics is unavoidable, as it can give much superior performance. The major impediment to the wide-use of photonics is the cost. Three major components that contribute to the cost escalation are the absence of integrable light source, fast modulator, and effective fiber to waveguide coupler.

The latest issue was addressed in this work. Coupling light efficiently from fiber to waveguide is challenging because of the size (6μm core diameter for fiber, 500nm for waveguide), shape, and refractive index (~1.5 for fiber, 3.5 for waveguide) differences. Optical solder was proposed as the gap filler in between the fiber and waveguide to account for the fabrication uncertainties. Together with an inverse taper structure patterned in the waveguide end, the coupling loss was much reduced from 7.5dB (direct butt-coupling), to less than 1dB. Besides, optical solder increases the reliability of device, as it prevents moisture and dust from impairing the optically active area of the die. Its fabrication is also integrable with the current CMOS technology. The configuration allows high density optical interconnect at the edges of the die; together with the electrical interconnect spreading across the area of the chip. All these make this system very good potential coupling method to solve one of the major impediments above, and thus enable the widespread use of electronic-photonic ICs.

Thesis Supervisor: Lionel C. Kimerling
Title: Thomas Lord Professor of Materials Science and Engineering

ACKNOWLEDGEMENTS

I would like to express my utmost gratitude to everyone who had helped and supported me towards the completion of this thesis. First of all, I would like to thank my advisor, Prof. Kimerling, who gave me the opportunity and trusted me to work on this project in the first place. He is truly an admirable figure; he has so many things under his hand, yet is able to have them all settled calmly.
I would also like to express a great thank-you to Winnie Ye, my very caring mentor. She continuously offers me ideas and kind guidance such that I'm motivated to proceed much further. Thank you very much!

I was highly indebted to Yip Chan Hoe, without him this thesis wouldn't have been possible. He helped me with the resources I needed for this work, from the installations to the troubleshooting, and gave me a lot of advices of how to survive through this taxing year. I won't be able to thank him enough here!

I am also very grateful to Prof Wong, Prof Chua, Naga, Kunal, Wardhana, Xiao Yan, Vibin, Yuyan, Luojia, and Zhang Liang, for all the time they had spared me for the discussions which had aided me much in understanding my thesis work here. Thanks a lot to Kwan Wee for all the info and help with the admin works. And to all my fellow SMA classmates, it had been fun to cramp in the athenaeum, each working with our own thesis, and shared the excitement and distress of our work during the tea times.

Last and foremost, to my dear parents and brothers, thank you so much for always being there at the times I needed most. Their sincerities are the utmost motivation for me to work hard and strive for the better.

CONTENTS

ABSTRACT **3**

ACKNOWLEDGEMENTS **4**

CONTENTS **5**

LIST OF FIGURES **7**

LIST OF TABLES **9**

Chapter 1 Introduction **10**
1.1 Background 10
1.1.1 The need for optics 10
1.1.2 Transceivers 11
1.1.3 Evolution of Integration Technology 12
1.1.4 Cost Drivers 14
1.2 Scope 14
1.3 Objectives 14
1.4 Thesis Outline 15

Chapter 2 State-of-Art Technology **16**
2.1 Taper-based Coupler 16
2.2 Grating-based coupler 17
2.3 Prism Coupler 18
2.4 Inverse-Taper Coupler 19
2.5 Other design 19
2.6 Proposed structure and Comparisons 20

Chapter 3 Theory **22**
3.1 Maxwell's Equations 22
3.2 Refractions and Reflections 23
3.3 Propagation in Single Mode Waveguide 25
3.4 Mode Field Diameter 26
3.5 TE and TM polarizations 27
3.6 Effective Index Method 27

Chapter 4 Simulations Resources **29**
4.1 Finite Difference Time Domain 29
4.2 Boundary Conditions 30

Chapter 5 Coupler Design & Simulation **31**
5.1 Design Parameters 31
5.2 Inversely-Tapered Waveguide 33
5.2.1 Effect of waveguide-end width 33
5.2.2 Effect of taper length 34
5.3 Optical Solder 35
5.3.1 Longitudinal Displacement – Comparison with those without optical solder. 35
5.3.2 Effect of Varying Optical Solder Refractive Index 36
5.3.3 Effect of Varying Optical Solder Shape 38
5.4 Effect of Vertical Misalignment 40
5.5 Crosstalk between two waveguides 41
5.6 Summary 42

Chapter 6 Application and Packaging **44**
6.1. Application: Optical Interconnect 44
6.2 The Package 47
6.2.1 Ball grid array (BGA) 47
6.2.2 Substrate modification 47
6.2.3 Flip Chip Processes 48
6.3 Materials for Optical Solder 50
6.4 Cost Analysis 54

Chapter 7 Conclusion **56**

References **57**

LIST OF FIGURES

Figure 1.1: Integrated Optoelectronics [1] 11
Figure 1.2: Receiver Optical Assembly (ROSA), Transmitter Optical Assembly (TOSA), and the general parts of TO-cans [2] 13
Figure 1.3: (a) Silicon optical bench approach [3], (b) Planar Lightguide Circuit where the optical functions such as waveguiding, wavelength filtering and/or mode-size converting are performed [2] 13
Figure 2.1: (a) Pseudo-vertical taper, (b) grayscale taper [5] 17
Figure 2.2: Dual grating-assisted directional coupler [8] 18
Figure 2.3: Silicon prism coupler [11] 18
Figure 2.4: Inverse-taper coupler [14] 19
Figure 2.5: Fiber-to-waveguide coupling scheme using large silicon block on top of a submicrometer dimensional silicon rib waveguide[7] 20
Figure 3.1: Refraction and reflection when light is incident on an interface [17] 24
Figure 3.2: Total internal reflection occurs when the incidence angle exceeds the critical angle 25
Figure 3.3: Light distribution in the fiber 26
Figure 3.4: Frame reference showing the two polarizations 27
Figure 3.5: (a) 3D structure to be collapsed to 2D for FDTD simulation, (b) Cross-sectional view –light propagates to x direction, with electric field aligned to y direction (E_y – TE polarized) 27
Figure 3.6: (a) Assuming infinite width of the core with height b, (b) Assuming finite width with infinite height of the core 28
Figure 4.1: Yee-cube 30
Figure 5.1: Buried silicon on insulator 31
Figure 5.2: Changes in effective index as a function of waveguide width 32
Figure 5.3: The 2D cells used for light coupling simulation; dash lines denote PML boundaries 32
Figure 5.4: Effect of waveguide-end width on coupling loss 34
Figure 5.5: (a) Effect of taper length on coupling loss (b) Ray optics picture explaining loss in the taper region 35
Figure 5.6: Effect of longitudinal displacement of fiber wrt to the waveguide w and w/o optical solders at h = 100um 36
Figure 5.7: Effect of optical solder index on the coupling loss 36
Figure 5.8: Illustration of light transmission in fiber interrupted by gap filled with optical solder with refractive index: (a) n = 1 (air), (b) n = 1.49265, and (c) n = 2.572 37

Figure 5.9: Simulation geometry – modifying the optical solder shape 38
Figure 5.10: Effect of optical solder shape at different gap distance on the coupling loss 39
Figure 5.11: Effect of varying optical solder shape at no waveguide inverse taper 40
Figure 5.12: Optimal solder-end width as a function separation distance H 40
Figure 5.13: Effect of Vertical Misalignment 41
Figure 5.14: Power distribution of two waveguides with and without optical solder 42
Figure 6.1: System architecture of a desktop PC [5] 44
Figure 6.2: Frequency gap between the microprocessor and FSB over the last 15 years [5] 45
Figure 6.3: (a) Mechanism of light coupling through microlenses interface, (b) Schematic view of the solder bumps and microlenses arrays [26] 46
Figure 6.4: Underfilling chip/PCB space 46
Figure 6.5: Fiber to waveguide butt coupling 46
Figure 6.6: Substrate modification to make groove and hole for the fiber and chip to sit on 47
Figure 6.7: Various flip chip processes [29] 48
Figure 6.8: (a) Optical solder coated fiber, (b) Chip placement into the hole with optical solder coated fiber in place, (c) side view of the fiber and chip in place 49
Figure 6.9: (a) Optical fiber, (b) Placement of fiber and chip on the groove and hole, (c) side view of the filled gap 50
Figure 6.10: Typical solder reflow profile [31] 52
Figure 6.11: Typical cost induced in making an integrated circuit [38] 54

LIST OF TABLES

Table 6.1: Mechanism of absorption at various wavelengths [30] 51
Table 6.2: Potential materials for optical solder 53

Chapter 1 Introduction

1.1 Background

1.1.1 The need for optics

As CMOS technology is scaled, it will become increasingly difficult for conventional copper interconnect to satisfy the bandwidth requirement due to increased power consumption, signal distortion, crosstalk and pin-out capacity. This is increasingly apparent as data rates exceed 1Gbps [1, 2]. High speed electronic transmission over copper is currently limited to distances around 100m, and this distance will certainly shrinks as data rates rise.

To overcome the limitations imposed by the electronic communication, optics has been introduced at longer distances in the form of an optical fiber. It is currently used for almost all high speed (> 1Gbps) interconnects running longer than 100m, and is competing in 1-100m commercial application.

Photonics has various advantages over copper wire that enable the migration of copper to optical fiber: capable of high capacity data rate up to 50 Tbps is possible using Wavelength Division Multiplexing (WDM), low loss ≈ 0.2 dB/km, low power requirement, electromagnetic interference (EMI) immunity, low crosstalk, low cost and maintenance.

Complete replacement of electronic components into the photonic ones is currently not possible, due to unavailability of some electronics-analog computational components in photonics. But it can be integrated with the electronics by replacing some major performance limiting components, i.e. the electronic interconnects, thus named optoelectronics.

1.1.2 Transceivers

To merge photonics into electronics, transceivers are used to convert photons into electrons and vice versa. Transceivers are transmitter and receiver packaged into a single device. Optical signals coming from fibers are received by the photodetector in the receiver. There, the signals are converted to electrical signal, and are then passed to the respective electronic circuitry for data processing. Similarly, electrical signals coming from this circuitry would trigger the laser in the transmitter and be modulated to generate the optical signal which will exit to the fiber for transmission.

The basic components in transceivers are the light source and modulator (in transmitter), photodetector, wavelength division multiplexer, and coupler (as receiver components).

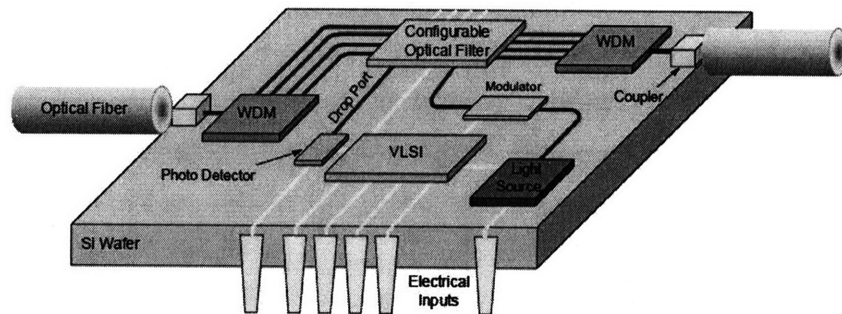

Figure 1.1: Integrated Optoelectronics [1]

Light source/Modulator

There are four types of light sources: (a) LED, (b) Fabry-Perot Laser, (c) VCSEL, and (d) DFB laser. They give different performances and are used in different applications. The modulation bandwidth of the light source determines the maximum data rate possible in the transceiver. For example, the modulation bandwidth of and LED is determined by carrier lifetime (2 - 5 ns), which translates into a maximum data rate of 1Gbps for LED light source. The modulation bandwidth of a laser diode is larger than an LED and is determined by laser power and photon lifetime in the cavity. Laser diodes can operate at 1Gbps, 10Gbps, and beyond.

Photodetector

A photodetector absorbs the photons from the optical signal and converts them to electric current. It can be made of Germanium which has good photodetector properties (small bandgap, large absorption coefficient, high quantum efficiency) grown on silicon, forming SiGe p-i-n photodiode. When photons with energy larger than the bandgap energy hit the photodetector, the electrons in the conduction band is excited to the valence band, creating electron-hole pair that generates current driven to the amplifier circuitry.

Wavelength Division Multiplexer (WDM) and Demultiplexer (DWDM)

To increase the data capacity carried in a single fiber, multiple wavelengths of light can be combined together from individual laser and modulator using WDM. When the multiple wavelengths of light reach the receiver, they will enter DWDM where light with different wavelengths will be separated into different waveguides and reach their own photodetector. The demultiplexing is done by using ring resonator, which is a waveguide with a close-loop shape. Only light with appropriate resonance frequency would be coupled into the ring.

Coupler

Light will be coupled from the fiber into the waveguide before being separated by the ring resonator. A single mode fiber has diameter of 6-10um, while the waveguide cross-section area is approximately 0.1um^2 (for Si waveguide). There is large mode size and shape difference which results in large coupling loss. A coupler is necessary as an intermediate medium between the fiber and waveguide to reduce the loss. The coupling methods will be discussed extensively in this report.

1.1.3 Evolution of Integration Technology

Box Level Transceiver – Discrete Components

Early generation of optical transceivers, and many of current commercial transceivers, are built based on discrete optoelectronic chips such as FP or DFB laser diodes (LD) and

PIN (p-intrinsic-n diode) or APD (avalanche photodiode) photodetector (PD) packaged individually in the transmit and receive TO-cans. These TO-cans are subsequently assembled into optical subassemblies (OSAs) and finally mounted onto printed circuit boards.

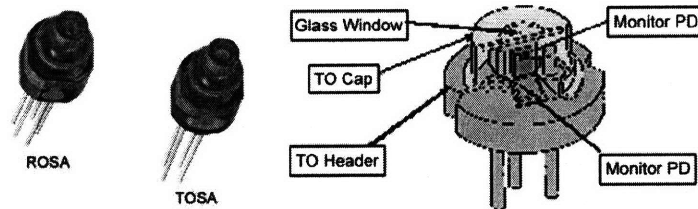

Figure 1.2: Receiver Optical Assembly (ROSA), Transmitter Optical Assembly (TOSA), and the general parts of TO-cans [2]

Board Level

In board level integration, the free space optic components, such as mirror and lenses, and TO-cans packaged in OSAs are replaced with planar lightguide circuit (PLC) being co-packaged with other photonic and microelectronic chips in a silicon bench. Optical functions, such as waveguiding, wavelength filtering and/or mode-size converting, etc, are performed by the PLC circuits. Consequently, the total number of the discrete optoelectronic components and the overall package size are reduced.

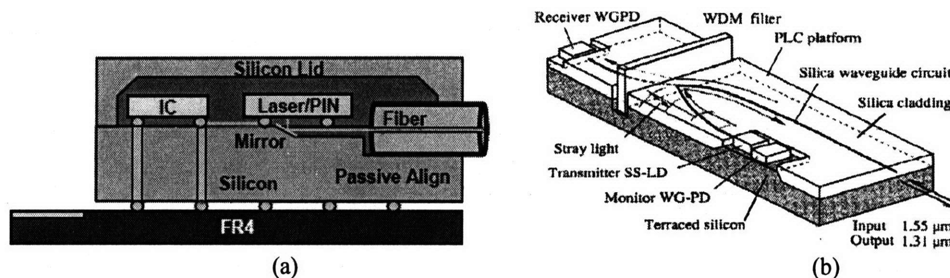

Figure 1.3: (a) Silicon optical bench approach [3], (b) Planar Lightguide Circuit where the optical functions such as waveguiding, wavelength filtering and/or mode-size converting are performed [2]

Chip level

In chip level integration, the photonic devices are connected either monolithically or hybrid on a silicon wafer together with the electronic driver and receiver circuitry to form

a single and rugged photonic/electronic integrated circuit. In hybrid approach, different materials used for light emitting materials are bonded to Si substrates where other electronics are built on. In monolithic approach, those materials are integrated by sequential deposition, growth and pattern transfer onto Si substrates, producing a complete set of optoelectronic functionalities [4].

1.1.4 Cost Drivers

Monolithic integration on silicon gives the lowest overall processing cost, but there are three major problems that impede its realization: light emission, fast modulation for data encoding and low coupling loss between optical fibers and silicon waveguides.

Silicon is not a good light emitter because it has indirect bandgap. Light emission from silicon is an indirect phonon mediated processes with low probability, and it has fast non-radiative transitions that severely prevent population inversion at high pumping rates needed to achieve amplification and lasing [4].

High coupling loss when signal comes in from the fiber to the waveguide would reduce the optical power delivered, which increases the bit error rate (BER) and finally the bandwidth.

1.2 Scope

This report focuses on the third major problem in realizing silicon based optoelectronic devices: light coupling from fiber to the waveguide. An optical solder material, combined with some feature on the waveguide, was proposed to mediate fiber and waveguide. The platform analyzed was Silicon-on-Insulator (SOI), where silicon is the guiding waveguide on chip.

1.3 Objectives

The objectives of this work were:

- To make engineering analysis on the feasibility of optical solder as fiber-to-waveguide coupler through simulations
- To suggest applications and the method to incorporate optical solder into CMOS processes
- To make a cost analysis of the incorporation of optical interconnect as compared to its electronics counterpart

1.4 Thesis Outline

The following chapter reviews the methods that have been used for fiber-to-waveguide coupling, continued with some theoretical treatment required to better understand the work in Chapter 3. Chapter 4 gives a brief description of the MIT Electromagnetic Equation Propagation (MEEP), which is the software used throughout this work for simulating the fiber-waveguide coupling. The results of simulations and the concluded optimal design are presented in Chapter 5. Chapter 6 presents the analysis of applications, fabrications, materials and the cost of using optical solder. All these are finally concluded in Chapter 7.

Chapter 2 State-of-Art Technology

As an integral part of optoelectronic devices, there has been a great deal of efforts done in order to obtain high coupling efficiency between fiber and waveguide. The coupling can be guided, where light is confined throughout from fiber to waveguide, or unguided, by using micro lenses to focus light into the small diameter waveguide.

As mentioned in Section 1.2, this thesis focus on the high index contrast material, as it has gained strong interest over the last decade. High index contrast does not have a strict definition, but roughly speaking, the ratio of the difference between the highest and the lowest refractive index in a device to their sum should be of the order of 50% or more before one can truly exploit the benefits of this high contrast.

HIC allows strong confinement of light of propagating mode to a very small cross-section and thus ultra-compact devices. It can be achieved by using a combination of a semiconductor material with a low-index dielectric or by a combination of a metal with a semiconductor or a dielectric. The most popular material system for HIC devices is silicon-on-insulator (SOI) system because of its manufacturability using CMOS-oriented technologies and thus allowing monolithic integration of optical and electrical functionality. Besides, SOI waveguides are virtually transparent to the optical communication wavelengths around 1550nm, which is very important to ensure reliable signal transmission. Several existing coupling methods are discussed next, and compared to the method in this work.

2.1 Taper-based Coupler

Pseudo-vertical tapering transforms a fiber mode to a rib waveguide mode using an overlying width taper, as shown in Figure 2.1(a). A horizontally tapered waveguide is patterned on top of another waveguide, and the optical mode is gradually squeezed from

the top taper to the smaller, lower waveguide [5]. This allows efficient coupling with insertion loss < 0.5dB [6] at taper length of 1mm.

The key parameters in this pseudo-vertical structure are the length of the taper and the taper tip width (see Figure). A longer taper length increases the coupling efficiency as it allows smoother mode transformation. The tip width, on the other hand, requires being as small as possible that there is almost no optical mode in the tip region [5]. The fabrication of this structure presents challenges, as the coupling is highly sensitive to the tip width and the overlying block requires a precisely controlled etch to the depth of the block, which approaches the limit of CMOS processing tolerances [7].

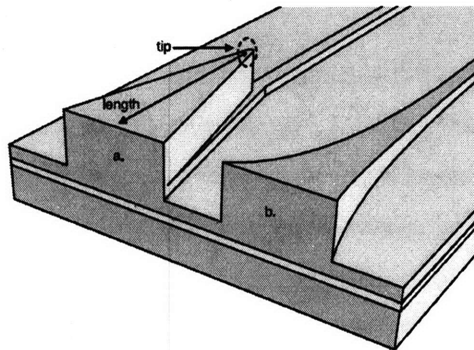

Figure 2.1: (a) Pseudo-vertical taper, (b) grayscale taper [5]

Grayscale taper coupler (Figure 2.1(b)) smoothly squeezing the large fiber mode'radius into the small waveguide mode. It should results in very low loss, but the grayscale based lithography adds some additional complexity and cost; the reticle alone is typically five times more expensive than a standard lithography reticle [5].

2.2 Grating-based coupler

Dual grating-assisted directional coupler was proposed [8] consisting two separation layers and three waveguides. The first waveguide was made of 5um thick SiON layer to receive the beam from the fiber; it has much lower refractive index than silicon resulting in lower back-reflections. This layer is separated to the next Si_3N_4 waveguide, which has refractive index in between the SiON and Si waveguide, by first separation layer with

grating formed at their interface (Figure 2.2) where the light from the first waveguide is coupled in. The second grating is formed between the second separation layer and the third, main silicon waveguide. This light guiding method is based on graded index [9, 10] to coupler the light from the top layer vertically down to the bottom silicon waveguide. Coupling efficiency as high as 90% could be achieved. However, this structure is polarization sensitive and its fabrication requires CMOS compatible processing [7].

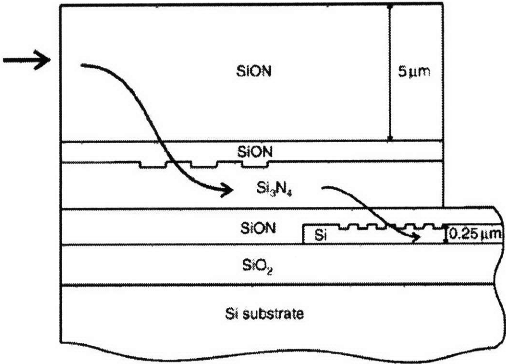

Figure 2.2: Dual grating-assisted directional coupler [8]

2.3 Prism Coupler

Lu and Prather [11] described a fiber to SOI waveguide coupling method utilizing total internal reflection within a silicon prism bonded to the waveguide layer. The maximum theoretical efficiency was 77% for TE polarized light. This method was based on a vertically tapered surface as the prism to reflect the light down to the waveguide, and thus requires expensive grayscale lithography. Besides, there is a small low index gap tunnel layer between the silicon prism and waveguide, which implies separate fabrication and bonding process that introduce more alignment issues.

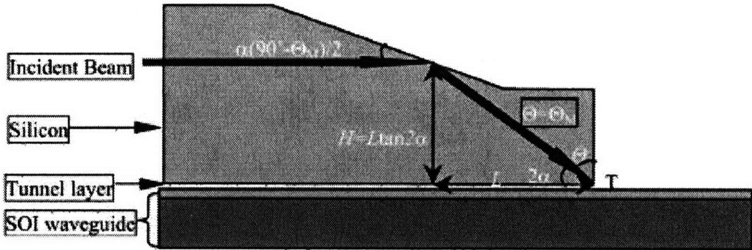

Figure 2.3: Silicon prism coupler [11]

2.4 Inverse-Taper Coupler

Instead of tapering the waveguide to end width of the fiber core, inverse-taper coupler consists of a waveguide tapered to a nanometer-sized tip at the facet in contact with the fiber. The purpose is to reduce the effect index of the waveguide gradually to match that of the fiber, such that the mode field profile becomes delocalized at the tip of the waveguide core and forced to reside in the cladding. The term inverse-taper generally refers to a laterally tapered waveguide (as shown in Figure 2.4), instead of the 3D inverse-taper [12], where fabrication is complicated as grayscale lithography is required. The small tip also results in negligible back-reflections because of this effective index matching. Mode-mismatch loss, as low as 0.5dB, was obtained for TE-like mode at taper length of 40um. The only drawback for this method is the fabrication which requires complexity of e-beam lithography to achieve the small tip width, but fabrication using CMOS processes has been demonstrated [13].

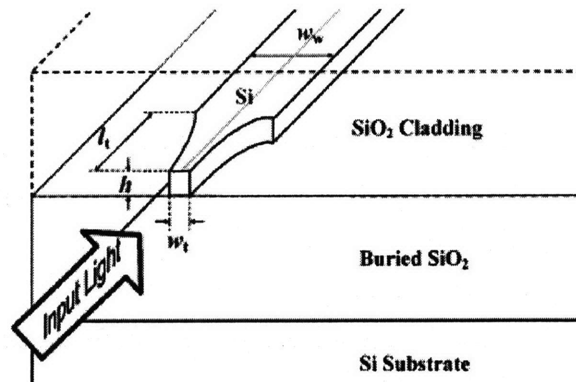

Figure 2.4: Inverse-taper coupler [14]

2.5 Other design

Doylend [7] reported a monolithically integrated fiber to SOI coupler by using relatively large silicon block on top of the silicon rib waveguide, as shown in Figure 2.5. Modifying the pseudo-vertical taper above, an oxide etch stop was incorporated between the overlying "block" and the rib waveguide. The mechanism is to excite two modes by the input, and these beat with each other to shift power from the top to the bottom silicon layer. The fabrication disadvantage in the pseudo-vertical taper, the taper tip, can now be discarded in favor of a lock of uniform width. Simulations of the structure showed that

>90% coupling efficiency could be maintained for all reasonable manufacturing tolerances for coupler length of 800um.

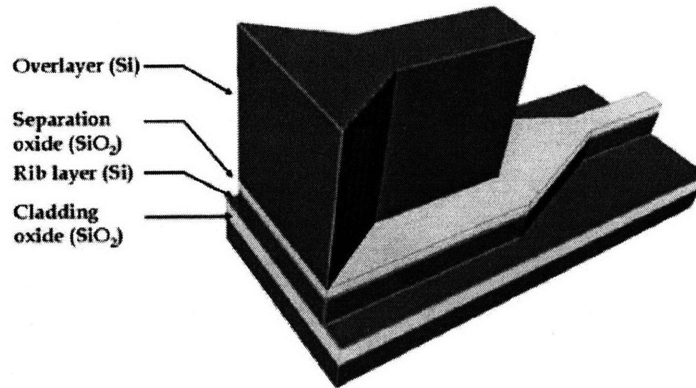

Figure 2.5: Fiber-to-waveguide coupling scheme using large silicon block on top of a submicrometer dimensional silicon rib waveguide[7]

Commercial fiber to waveguide coupler in device currently utilizes unguided coupling method: microlenses, which are fabricated on top of the structure. The light from the fiber shines on the microlenses from the top of the device. The microlenses then focus the light to a small spot on the silicon waveguide.

2.6 Proposed structure and Comparisons

Among the coupling methods reviewed, inverse-taper structure is the simplest and can be easily fabricated by the industry CMOS process. Other methods would require multiple patterning and etching steps, even compounded by bonding steps in some method. Besides, the mode mismatch loss can be <10% at just a length of 40um, as compared to other methods that can hit a length requirement of 1mm, thus facilitates continuous miniaturization of silicon optoelectronic functions [13].

In this thesis, coupling method utilizing both the inverse taper and 'optical solder' is analyzed. Optical solder with matching effective index is placed in between the fiber and the inversely-tapered waveguide. As implies, the ability to utilize CMOS processes for the fabrication is very desirable for technology adoption. Optical solder is used to fill the gap between the fiber and waveguide to overcome to the fabrication inaccuracies, i.e. it

increases the misalignment tolerance in the longitudinal direction, and reducing the surface roughness sensitivity of both the fiber and waveguide facets. Besides, the optical solder increases the device reliability, as the coupling won't be affected by external defects, such as dust.

Chapter 3 Theory

This chapter reviews some physics to better understand the results to be presented in the chapters to come.

3.1 Maxwell's Equations

A set of four Maxwell's equations gives a complete description of the production and interrelation of the electric and magnetic fields.

- Electric fields are produced by changing magnetic fields

$$\vec{\nabla}\times\vec{E} = -\frac{1}{c}\frac{\partial\vec{B}}{\partial t} \quad \text{.................. (3.1)}$$

- Circulating magnetic fields are produced by electric currents and by changing electric fields:

$$\vec{\nabla}\times\vec{H} = \frac{4\pi}{c}\vec{J} + \frac{1}{c}\frac{\partial\vec{D}}{\partial t} \quad \text{........... (3.2)}$$

- Electric field diverges from electric charge:

$$\vec{\nabla}\cdot\vec{D} = 4\pi\rho \quad \text{...................... (3.3)}$$

- There are no isolated magnetic poles:

$$\vec{\nabla}\cdot\vec{B} = 0 \quad \text{.......................... (3.4)}$$

, where $\vec{E}$ and $\vec{H}$ are electric and magnetic fields, $\vec{D}$ and $\vec{B}$ are the displacement and magnetic induction fields, ε is the dielectric function. $\vec{J}$ is free current density and ρ is the free charge density. All of these are potentially functions of both the position $\vec{r}$ and the time t. And finally c is the speed of light in vacuum.

In optics, only the case where no free charge or current is the subject of interest, so both $\vec{J}$ and ρ are zero [15]. Besides, several assumptions were made to solve the equations:

1. The system has a linear response to electromagnetic (EM) radiation, i.e. ε is independent of $\vec{E}$, which translates to $\vec{D}=\varepsilon\vec{E}$
2. There's no frequency dependence of dielectric function and ε is a real number (any absorption of light the material is neglected)
3. Magnetic permeability is assumed to be unity, which implies that $\vec{B}=\vec{H}$

Substituting these into (3.1) and (3.2), a wave equation in terms of the magnetic field can be obtained:

$$\vec{\nabla}\times\frac{1}{\varepsilon}\vec{\nabla}\times\vec{H}=-\frac{1}{c^2}\frac{\partial^2\vec{H}}{\partial t^2} \text{ .... (3.5)}$$

A solution to this equation in terms of harmonic modes:

$$\vec{H}(\vec{r},t)=\vec{H}(\vec{r})e^{-i\omega t} \text{ .... (3.6)}$$

, where ω is an angular frequency, will simplify the equation by dropping the time variable in (3.5):

$$\vec{\nabla}\times\frac{1}{\varepsilon(\vec{r})}\vec{\nabla}\times\vec{H}(\vec{r})=\left(\frac{\omega}{c}\right)^2\vec{H}(\vec{r}) \text{........ (3.7)}$$

This is Maxwell's master equation to obtain $\vec{H}(\vec{r})$. The electric field can then be recovered by using:

$$\vec{E}(\vec{r})=\frac{i}{\omega\varepsilon_0\varepsilon(\vec{r})}\vec{\nabla}\times\vec{H}(\vec{r}) \text{.............. (3.8)}$$

3.2 Refractions and Reflections

When light enters a material with different refractive index to that it is traveling at, it will either be slowed down or speeded up. This result in the bending of light called refraction. Snell's law is a well-known formula to describe the bending of light in refraction. It says that the refracted ray lies in the plane of incidence; the angle of refraction θ_2 is related to the angle of incidence θ_1 by [16]:

$$n_1\sin\theta_1=n_2\sin\theta_2 \text{ .... (3.9)}$$

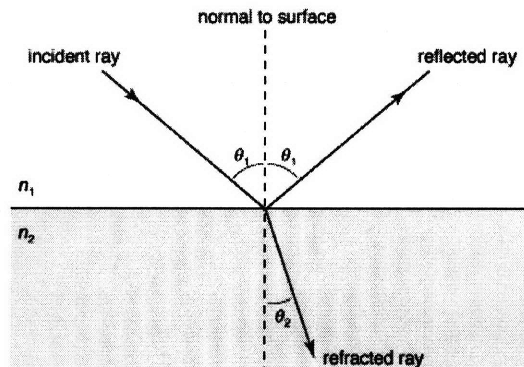

Figure 3.1: Refraction and reflection when light is incident on an interface [17]

Besides refraction, some portion of the light will be reflected at the same opposite angle of the incident one, known as Fresnel reflection. Reflection coefficient, R, is the fraction of intensity of the light that is reflected from the interface. R is polarization dependent, given by:

$$R_s = \left[\frac{\sin(\theta_t - \theta_i)}{\sin(\theta_t + \theta_i)}\right]^2 = \left[\frac{n_1\cos(\theta_i) - n_2\sqrt{1-\left(\frac{n_1}{n_2}\sin(\theta_i)\right)^2}}{n_1\cos(\theta_i) + n_2\sqrt{1-\left(\frac{n_1}{n_2}\sin(\theta_i)\right)^2}}\right]^2 \quad \text{..... (3.10)}$$

$$R_s = \left[\frac{\tan(\theta_t - \theta_i)}{\tan(\theta_t + \theta_i)}\right]^2 = \left[\frac{n_1\sqrt{1-\left(\frac{n_1}{n_2}\sin(\theta_i)\right)^2} - n_2\cos(\theta_i)}{n_1\sqrt{1-\left(\frac{n_1}{n_2}\sin(\theta_i)\right)^2} + n_2\cos(\theta_i)}\right]^2 \quad \text{.... (3.11)}$$

where R_s and R_p are the perpendicular and parallel polarization respectively.

If the light is incident on the interface at near-normal angle ($\theta_1 \approx \theta_2 \approx 0$), the reflection coefficient is given by:

$$R = R_s = R_p = \left(\frac{n_1 - n_2}{n_1 + n_2}\right)^2 \quad \text{......................... (3.12)}$$

, and the percent of transmission can be obtained easily: $\%T = 100(1-R)$.

Total Internal Reflection (TIR)

When light passes through an interface from high dielectric index (n_2) to the lower one (n_1) at the other side, the light beam is bent away from the normal, and thus the exit angle is greater than the incident angle. The exit angle will finally approach 90° with respect to the normal plane at an angle, which is termed the critical incident angle θ_c. Beyond this angle, the incident light will be totally reflected as shown in Figure 3.2. This is the principle of the light traveling in a single mode fiber, discussed in the next section.

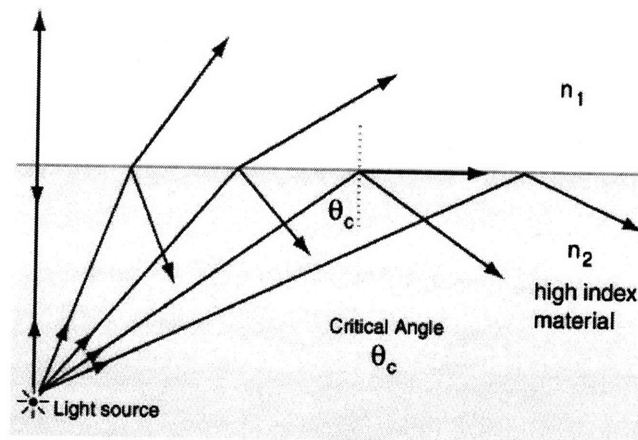

Figure 3.2: Total internal reflection occurs when the incidence angle exceeds the critical angle

3.3 Propagation in Single Mode Waveguide

Any structure that can guide light by restricting the spatial region is a waveguide. Optical fiber is circular waveguide made of silica which is used in the optical communication systems. It contains a region of increased refractive index (core) than its surrounding (cladding) such that TIR occurs at the interface to guide the light along the fiber.

There are two parameters that determine the characteristics of the signal propagation: attenuation and dispersion. Specifically, data is transmitted by a sequence of pulses; the system must ensure these pulses are received with a sufficiently low probability of error, also called the bit-error rate (BER). Given a particular receiver, achieving a specified BER requires a minimum received power and a maximum data rate or signal bandwidth [18]. Attenuation tends to increase the power required for the transmitter to meet the power requirement of receiver, while dispersion limits the bandwidth of data which may

be transmitted over the fiber. Interested reader is referred to [18] for deeper treatment on attenuation and dispersion.

Attenuation can be reduced by choosing the appropriate fiber material and refining the fabrication process, such that there is reduced energy absorption/scattering. Dispersion can be much reduced by using single mode fiber, i.e. a fiber that carries only a single ray of light (mode). Suppression of higher order modes can be done by choosing the appropriate core (n_{core}) and cladding ($n_{cladding}$) refractive indices, and the diameter of the fiber core (a). As a guideline, the fiber is single-mode if the normalized frequency, V, is smaller than 2.405.

$$V = \frac{2\pi a}{\lambda}\sqrt{(n_{core}^2 - n_{cladding}^2} \text{ .... (3.13)}$$

3.4 Mode Field Diameter

A beam of light does not have strict cross-sectional boundaries. Observing a cross-sectional beam's structure, it can be seen that a beam is most intense in the center, with its intensity declining gradually from the center outward. Mode field diameter (MFD) is a used to compare different Gaussian beams. It is a measure of the beam width when its intensity drops to $1/e^2 = 0.135$ of its peak value. It can be estimated by the following equation:

$$MFD = 2a\left(0.65 + \frac{1.619}{V^{1.5}} + \frac{2.879}{V^6}\right) \text{....... (3.14)}$$

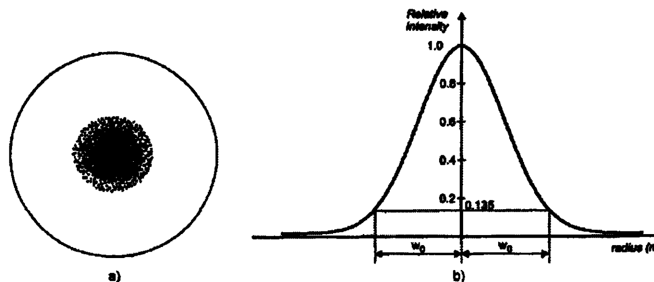

Figure 3.3: Light distribution in the fiber

3.5 TE and TM polarizations

Polarization is a property of waves that describe the orientation of their oscillations [19]. For 2D system, two types of polarizations can be identified: transverse electric (TE), and transverse magnetic (TM) polarizations. TE polarization has its electric field vector in-plane perpendicular to the direction of light propagation, while TM polarization has its electric field vector pointing out of the plane, also perpendicular to the direction of light propagation. In 2D slab system (3D-like system with a constant finite height), as shown in Figure 3.4, the polarization of light in the waveguide is not strictly TE or TM, but rather a majority of one with the balance of the other [1]. They are termed TE-like and TM-like modes instead.

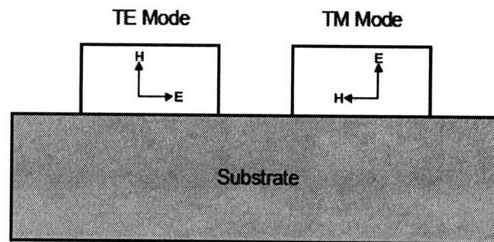

Figure 3.4: Frame reference showing the two polarizations

3.6 Effective Index Method

When a three dimensional structure is to be collapsed to two-dimensional structure, the refractive index used would be different from its real 3D index. A simple way to calculate its 2D 'effective index' is to use Effective Index Method (EIM). The structure of interest in this work is buried waveguide in Figure 3.5.

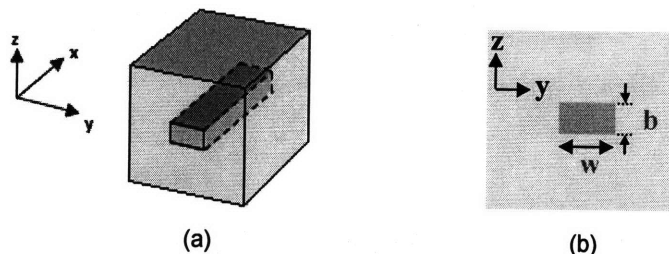

Figure 3.5: (a) 3D structure to be collapsed to 2D for FDTD simulation, (b) Cross-sectional view – light propagates to x direction, with electric field aligned to y direction (E_y – TE polarized)

The buried waveguide is initially approximated as a slab waveguide with height *b* (Figure 3.6a) to find $n_{eff,g}$, using the equation [20]:

$$k_o b\sqrt{n_{core}^2 - n_{eff,g}^2} = 2\tan^{-1}\left(\frac{\sqrt{n_{eff,g}^2 - n_{cladding}^2}}{\sqrt{n_{core}^2 - n_{eff,g}^2}}\right) + m\pi \quad \text{.....................} (3.15)$$

, where $k_0 = \frac{2\pi}{\lambda}$, and $m = 0$ assuming fundamental mode only.

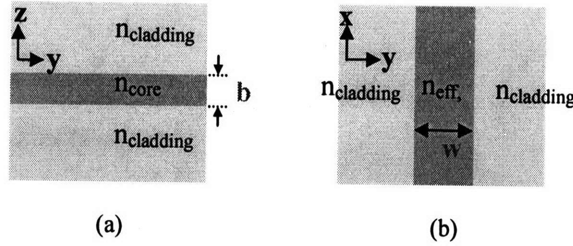

(a) (b)

Figure 3.6: (a) Assuming infinite width of the core with height b, (b) Assuming finite width with infinite height of the core

Using the calculated $n_{eff,g}$, the effective index of the 3D structure is approximated by another slab waveguide (Figure 3.6b):

$$k_o n_{eff,g} w\cos\theta_g = 2\tan^{-1}\left(\frac{\sqrt{\left(\frac{n_{eff,g}}{n_{cladding}}\right)^2 \sin^2\theta_g - 1}}{\left(\frac{n_{cladding}}{n_{eff,g}}\right)\cos\theta_g}\right), \text{ to solve for } \theta_g \quad .... (3.16)$$

and $n_{eff,TE} = n_{eff,g}\sin\theta_g$ to get the effective index of the 3D structure.

Chapter 4 Simulations Resources

Freely available simulation software, MIT Electromagnetic Equation Propagation (MEEP) developed by an MIT group, was utilized in this work. MEEP is a finite-difference time-domain (FDTD) simulation software package with subpixel smoothing for increased accuracy to model electromagnetic systems [21].

4.1 Finite Difference Time Domain

FDTD method belongs in the general class of grid-based differential time-domain numerical modeling methods [22]. Space is divided into a discrete grid and then the fields are evolved in time using discrete time steps. As the grid and time steps are made finer and finer, this becomes a closer and closer approximation for the true continuous equations, and many practical problems can be solved essentially exactly.

Examining Maxwell's equations (Eq (3.1) – Eq (3.4)), it can be referred that the change in the electric field (***E***) in time is dependent on the change in the magnetic field (***H***) across the space (the curl). As described above, FDTD time-stepping relation can be applied, i.e. at any point in space, the updated value of the ***E*** in time is dependent on the stored value of the ***E*** and the numerical curl of the local distribution of the ***H*** in space. The magnetic field is time-stepped in a similar manner. At any point in space, the updated value of the ***H*** in time is dependent on the stored value of the ***H*** and the numerical curl of the local distribution of the ***E*** in space. Iterating the ***E*** and ***H*** updates results in a marching-in-time process wherein the data of the continuous electromagnetic waves under consideration propagate in numerical grid stored in the computer memory.

However, when multiple dimensions are considered, the numerical curl calculation becomes complicated. This problem is simplified by using Yee algorithm [23], where the vector components of the ***E*** and ***H*** is staggered spatially about rectangular unit cells of a

Cartesian computational grid so that every ***E*** component is surrounded by four circulating ***H*** components and vice versa. In effect, Yee algorithm simultaneously simulates the pointwise differential form and the macroscopic integral form of Maxwell's equations. The latter is extremely useful in specifying field boundary conditions and singularities [24].

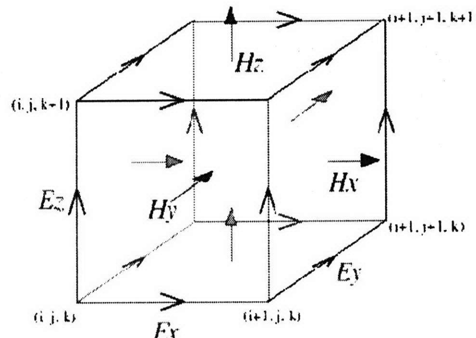

Figure 4.1: Yee-cube

Due to time and infrastructure limitation, only 2D simulations were performed. This was sufficient to give an understanding on the phenomena obtained by varying variables, and thus analogy can be drawn in its 3D space.

4.2 Boundary Conditions

In MEEP, there are three types of boundary conditions supported: Bloch-periodic boundaries, metallic walls, and PML (Perfectly Matched Layers) absorbing layers. Bloch-periodic boundaries are used in periodic structure, where one expects the computation to be extended periodically over some dimension. Metallic walls are simple boundary condition where the fields are forced to be zero on the boundaries as if the cell were surrounded by a perfect metal. Lastly, if one would like the boundaries to absorb all waves incident on them with no reflections, PML is used. The latest boundary condition is used throughout the work here.

Chapter 5 Coupler Design & Simulation

High coupling efficiency, simplicity of fabrication, high tolerance to misalignment, high packaging density, mechanical robustness and low materials costs are desirable characteristics of a coupler. Couplers that make use of optical solder to interface the fiber and the waveguide on chip was studied. The optical solder is made of polymer materials (Section 6.4) that can flow and be cured at elevated temperature to join the fiber and waveguide. The waveguide end is inversely-tapered to increase the efficiency. This chapter will present step by step design and simulations that confirm the technical feasibility of such coupling method.

5.1 Design Parameters

The SOI structure to be analyzed is shown in Figure 5.1. Silicon waveguide (n=3.5, 500nm x 220 nm) were embedded inside the SiO_2 cladding (n=1.49265, assumed to extend infinitely in x and y direction).

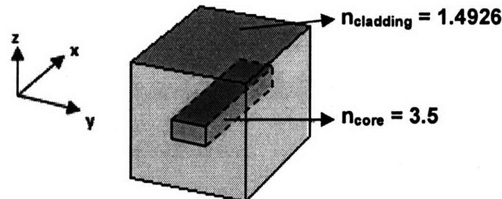

Figure 5.1: Buried silicon on insulator

Since only two dimensional FDTD simulations were available, the above 3D structure was collapsed to 2D using EIM method to obtain the effective index of the waveguide as described in Section 3.6. Only the TE mode was analyzed as it is more lossy as compared to the TM mode [25].

An effective index ($n_{eff,TE}$) of 2.52735 was obtained for the waveguide. The effective index of the taper region varies as the width decreases towards the waveguide end (Figure 5.2), but for simplification, the same effective index ($n_{eff,TE}$) is also used in the taper

region. This simplification was proven acceptable by simulation, i.e. by dividing a 30um taper length by 25 small blocks, each with increasing block width and corresponding effective index obtained in Figure 5.2. The coupling efficiency obtained increases by ~3% compared to that of homogenous index of 2.52735, which is an acceptable tolerance.

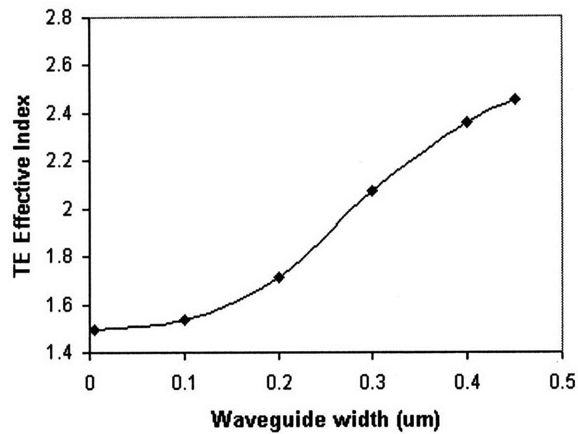

Figure 5.2: Changes in effective index as a function of waveguide width

Figure 5.3 shows the overall simulation geometry for the coupling simulation. Two computational cell sizes were used depending on the feature size of interest: 128x32 and 256x32, which corresponds to 128um x 32um and 256um x 32um area dimension[1].

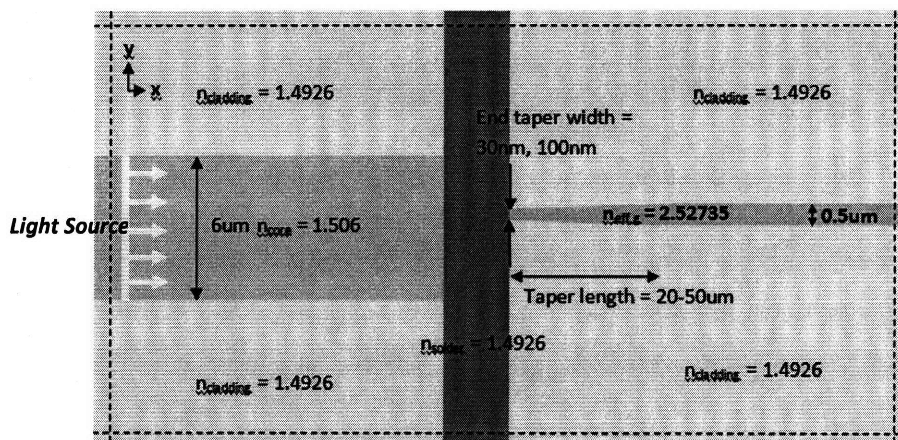

Figure 5.3: The 2D cells used for light coupling simulation; dash lines denote PML boundaries

[1] In fact, the bigger cell size results in up to ~5% coupling efficiency increase in accuracy, but at the expense of much longer simulation time

Perfectly matched layers (PML, Section 4.2) were used at the boundary of the computational cell to avoid boundary reflections. A TE Gaussian source with the width of the fiber core is placed to the right of the PML boundary.

Coupling Loss Measurement

Transmissions were measured by placing several lines along the fiber and waveguide where the light fluxes were measured. A fiber-only structure was simulated first to obtain the reference flux, followed by adding in the waveguide and features. The transmission was calculated by:

$$T = \frac{P_{\text{coupling}}}{P_{\text{reference}}} \quad \text{.....................} \quad (4.1)$$

The transmission percentage was converted to loss (dB) by:

$$Loss(dB) = -10 \times \log T \quad \text{.........} \quad (4.2)$$

Intrinsic coupling loss can be due to mode overlap mismatch, interfacial back-reflections, and scattering loss (e.g. in the taper region).

5.2 Inversely-Tapered Waveguide

5.2.1 Effect of waveguide-end width

The width of the waveguide-end is decreased towards the fiber in an inversely tapered waveguide (Section 2.4). The optimal end-width used for this work was concluded from the result in Figure 5.4, which shows that the decrease in coupling loss levels off at about w = 0.05um, i.e. further reduction in the waveguide end-width results in negligible reduction in coupling loss. Coupling loss as low as 0.86dB was obtained for end width = 50nm and taper length = 100μm, which corresponds to 82% transmission. Since bigger feature size is desirable process-wise, the taper width is fixed at 0.03um, which covers both over- and under-etch error.

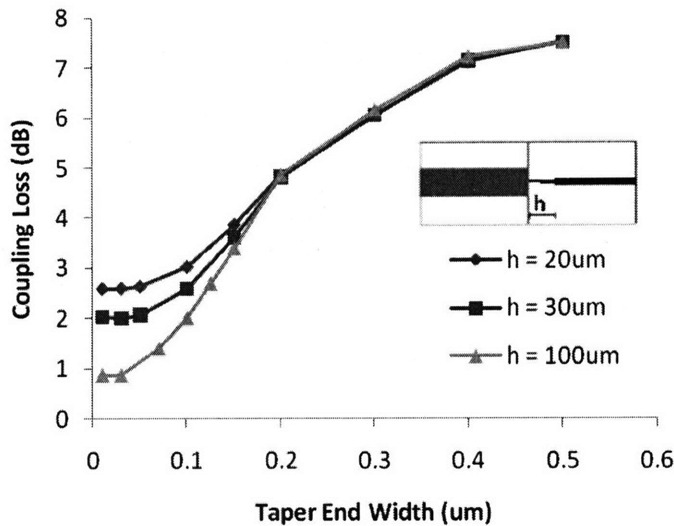

Figure 5.4: Effect of waveguide-end width on coupling loss

By varying the end-width, the mode size at the tip of the waveguide is varied. The larger the mode overlap between the tip and the waveguide, the larger the fraction of light which is coupled into the waveguide. Theoretically the effective index of the waveguide in the taper region decreases as the width decreases. It finally approaches the index of the fiber which increases the mode overlap between the waveguide and fiber. There is a fundamental mode mismatch loss during the coupling, other than small reflection occurring at the interface, i.e. the coupling efficiency does not increase with further decrease in taper end width. This should be due to the scattering occurring at the fiber/waveguide interface that causes the wavefront exiting the fiber to have oblique propagation angle relative to the fiber axis which reduces the mode overlap between the fiber and waveguide.

5.2.2 Effect of taper length

The next important taper waveguide parameter is the taper length, which affects the angle light travels in the waveguide taper region. Increasing the taper length allows adiabatic mode transformation that result in lower coupling loss. The change in coupling efficiency as a function of the taper length is shown in Figure 5.5 at two waveguide-end-width.

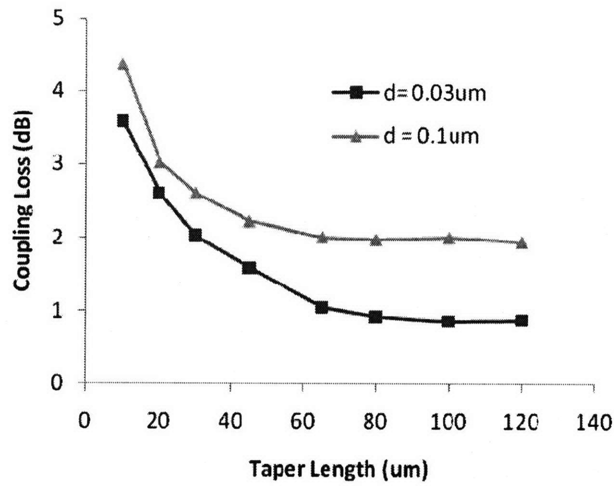

Figure 5.5: (a) Effect of taper length on coupling loss (b) Ray optics picture explaining loss in the taper region

Similar with the taper end width trend, the reduction in coupling loss does not increase much further when taper length is >60-80um. In ray optics, this can be projected as the light being totally reflected above its critical angle in the taper region when the taper angle is small enough.

One can see a clear trade-off by using long taper length: It offers higher coupling efficiency, but on the other hand, increases the footprint that opposes the miniaturization trend. Taper length of 30um, 50um, and 75um were analyzed further.

5.3 Optical Solder

5.3.1 Longitudinal Displacement – Comparison with those without optical solder

During the fiber-chip assembly process, there can be coupling loss due to the longitudinal displacement of the fiber with respect to the waveguide, especially when passive alignment is used where there is no constraints in longitudinal direction. Figure 5.6 shows how much the coupling loss if aggravated by the longitudinal displacement of fiber with respect to the waveguide, and the effect of optical solder present in this gap on the coupling loss. The optical solder here is assumed to be block, which covers the entire gap between the fiber and waveguide, extending to the height of fiber cladding.

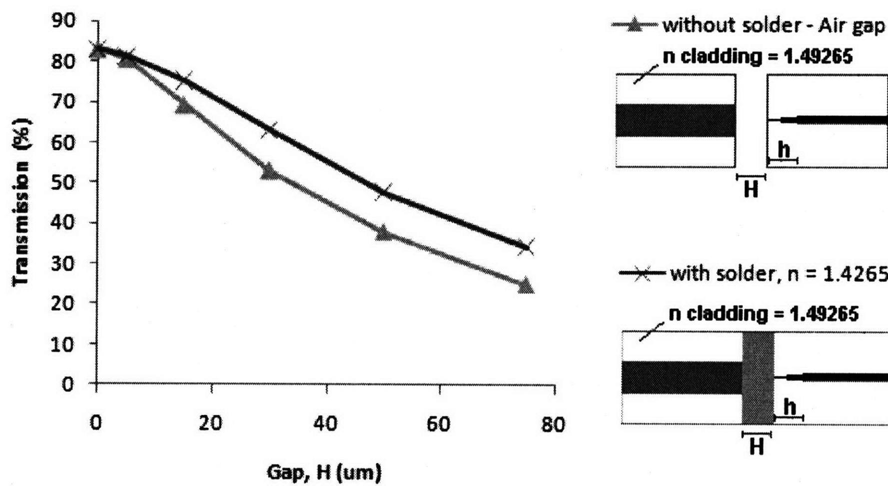

Figure 5.6: Effect of longitudinal displacement of fiber wrt to the waveguide w and w/o optical solders at h = 100um

In general, optical solder improves the coupling efficiency as the longitudinal displacement increases. At taper length of 100um (Figure 5.6), the efficiency improves by 10% at H>30um.

5.3.2 Effect of Varying Optical Solder Refractive Index

Varying the optical solder refractive index does not affect the coupling loss significantly; this is shown in Figure 5.7. There is only ~5% change in the coupling efficiency when the solder index is increased from n = 1.49265 to n = 2.69.

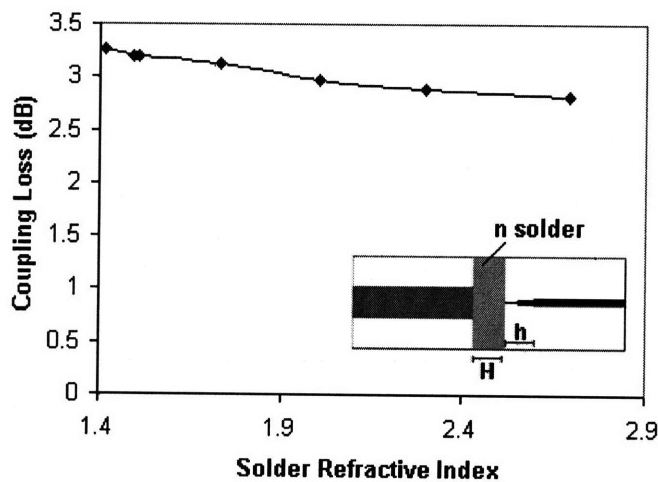

Figure 5.7: Effect of optical solder index on the coupling loss

Figure 5.8 shows the comparison of light travelling from fiber – optical solder – fiber, at three different solder indexes. Light incident on both the left and right fiber facet will be reflected and scattered to some degree. It is indeed true that the reflection loss caused by higher-index solder is larger, but looking at the interface refraction: $n_1 \sin\theta_1 = n_2 \sin\theta_2$, higher index solder gives smaller scattering angle, resulting in most transmitted power directed in to the center of the incident light path.

On the other hand, lower index solder (thus matching the fiber) results in less reflection loss, but the light is scattered to wider angle when it reaches the right fiber. The net result is lower power propagating in the fiber core (more is scattered to the fiber cladding).

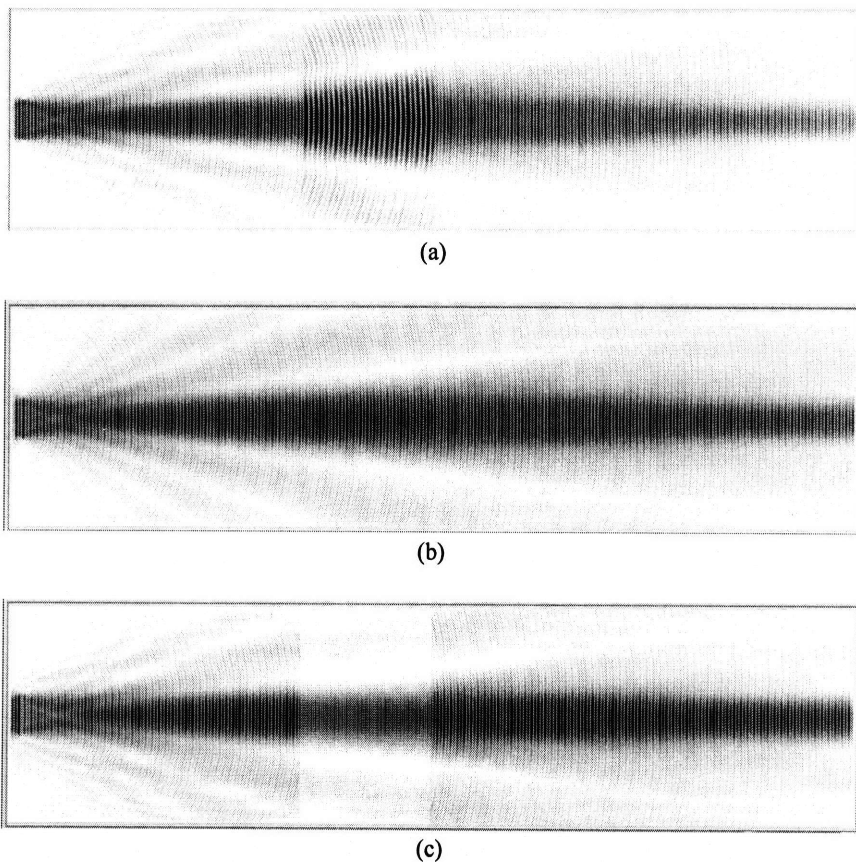

Figure 5.8: Illustration of light transmission in fiber interrupted by gap filled with optical solder with refractive index: (a) n = 1 (air), (b) n = 1.49265, and (c) n = 2.572

5.3.3 Effect of Varying Optical Solder Shape

Instead of covering the whole gap between the fiber and waveguide, the optical solder was assumed to have taper shape with 6um width, matching that of fiber core diameter, attached to the fiber side, and variable width *t*, attached to the waveguide side, as shown in Figure 5.9.

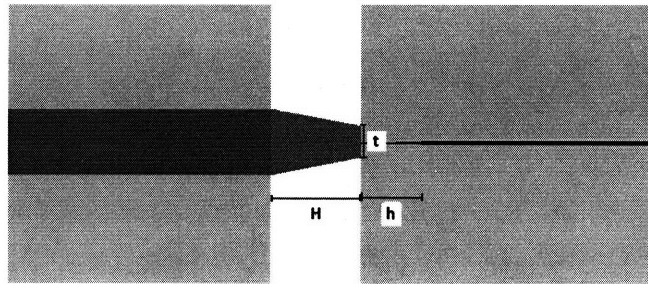

Figure 5.9: Simulation geometry – modifying the optical solder shape

Very big improvement in coupling efficiency can be obtained for very short waveguide taper length (Figure 5.10 a-c). E.g. for gap H = 20um, waveguide end width h = 30um:

- If no optical solder were used, the coupling loss is 3.88dB
- If block optical solder were used, coupling loss = 3.2dB
- The maximum coupling loss at various fiber end width is 2.08dB, which is much lower than that obtained with block optical solder
- The minimum coupling loss obtainable = 0.66dB

However, the efficiency of this system is very sensitive to the solder end-width.

Reverse to intuition, the coupling efficiency is much improved with short inverse-taper in the waveguide side instead of that with longer inverse taper length. However, no waveguide inverse taper at all is also not good (Figure 5.11), since at bigger solder-end width (which is more possible), the coupling loss is at the high side.

The optimal fiber-end-width varies at different fiber/waveguide gap, it increases with increasing H, shown in Figure 5.12.

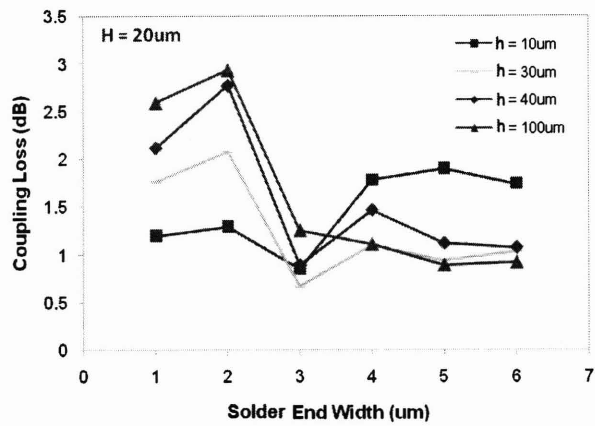

(a)

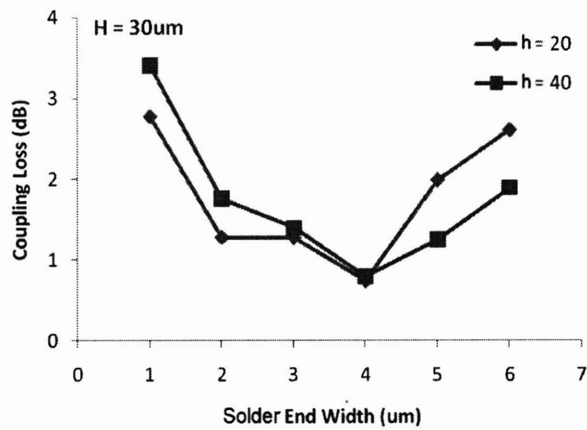

(b)

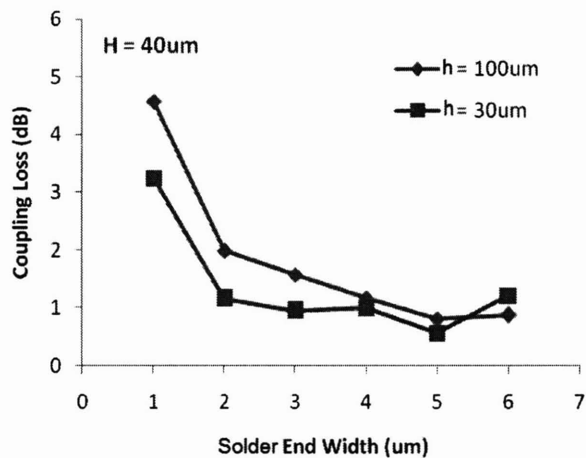

(c)

Figure 5.10: Effect of optical solder shape at different gap distance on the coupling loss

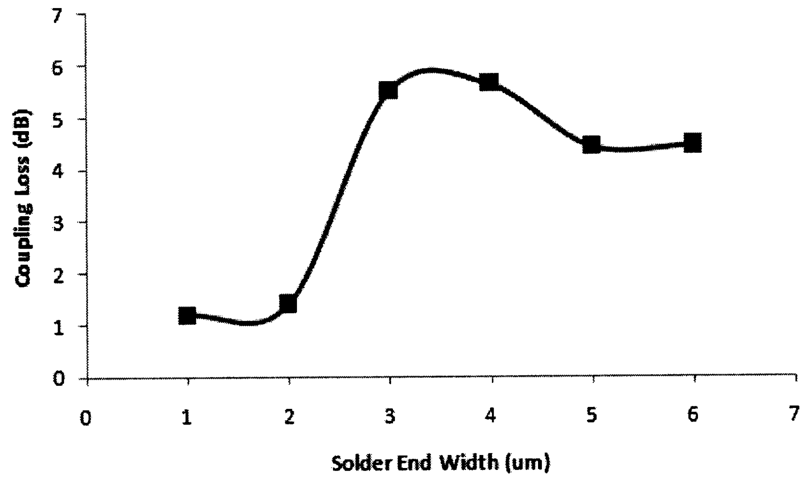

Figure 5.11: Effect of varying optical solder shape at no waveguide inverse taper

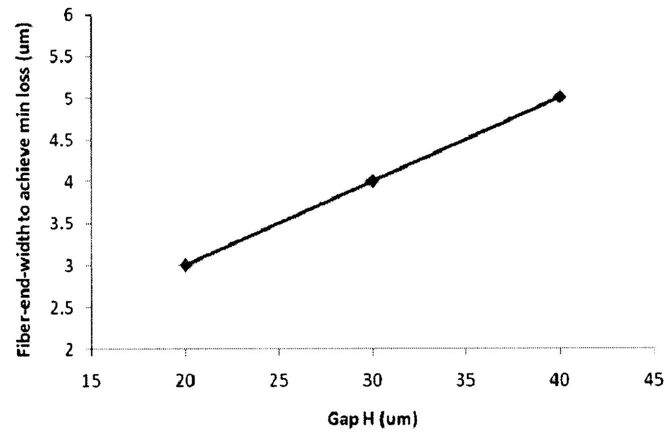

Figure 5.12: Optimal solder-end width as a function separation distance H

5.4 Effect of Vertical Misalignment

The waveguide axis was displaced by Δy from the fiber axis. It is seen in Figure 5.13, the tolerance to vertical misalignment is not improved by using optical solder, as the coupling loss with and without optical solder is nearly the same. There is no more coupling when the waveguide is 20um (y-direction) displaced from the fiber.

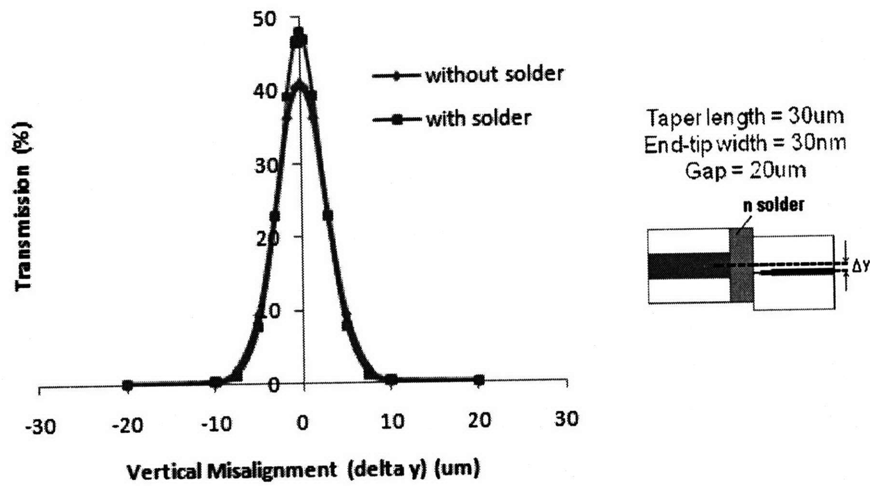

Figure 5.13: Effect of Vertical Misalignment

5.5 Crosstalk between two waveguides

We are interested to know the distance at which we can place two waveguides together to achieve reliable signal transmission. A second waveguide is placed besides the first one at a varying spacing of Δy, keeping the first waveguide fixed in place. The simulation geometry and parameters are shown in Figure 5.14a.

As seen in the result in Figure 5.14b, there is almost a 50-50 power distribution in the two waveguides when Δy ~ 1um. Beyond Δy = 3um, the power in waveguide 1 has reached the maximum possible transmission, but there's still quite high coupling into waveguide 2.

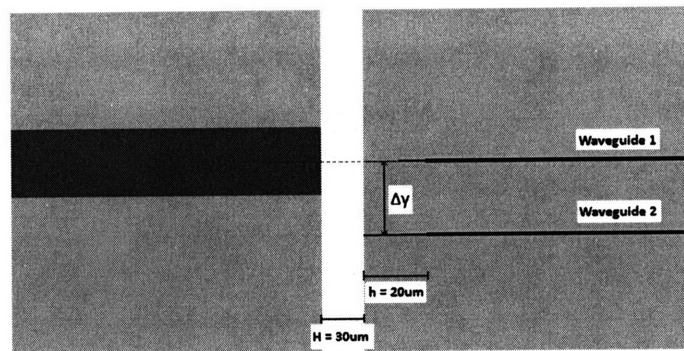

(a)

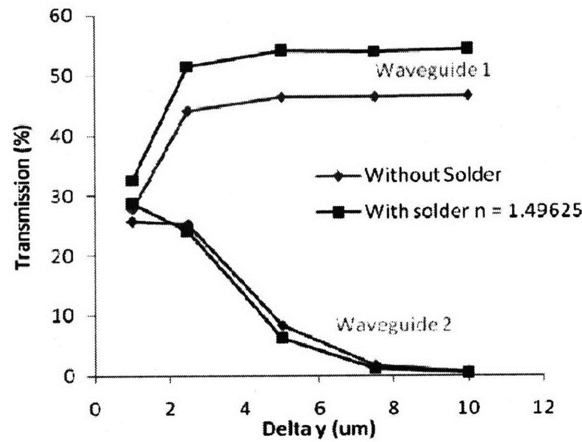

(b)

Figure 5.14: Power distribution of two waveguides with and without optical solder

5.6 Summary

The results of the simulations are summarized in Table 5.1.

Inverse Taper			
Variable	*Value (μm)*	*Coupling Efficiency (%)*	*Coupling Loss (dB)*
End tip width	≤ 0.05	82	0.86
Taper Length	≥ 100		
Optical Solder			
Variables		*Advantage?*	*Efficiency (%)*
Misalignment	Vertical	Yes	Depends
Tolerance	Horizontal	Yes	Up to 10%
Refractive index insensitivity		Yes	Within 5%
Crosstalk		No	-

Table 5.1: Summary of simulation results

Combining optical solder with inverse-taper waveguide, the coupling loss can be reduced considerably, from ~7.5dB when the fiber is directly butt-coupled into waveguide, to less than 1dB loss, at taper length < 100um, and end width waveguide taper of < 50nm, which poses no problem to the current industrial processes.

Although optical solder does not improve the vertical tolerance to misalignment, it improves the longitudinal tolerance up to 10%. Refractive index variation is not key issue

in the application to the coupling; optical solder with refractive index ~ 1.5 (that of fiber) can be safely adopted in order to account for fabrication facet roughness, i.e. optical solder reduces the sensitivity to fiber surface roughness.

Another key advantage of optical solder is the reliability during the application. Optical solder fully shielded the fiber/waveguide interface, and thus, no dust or impurities can interfere during the lifetime of the system, which is not the case when mirrors/lenses are used.

Chapter 6 Application and Packaging

6.1. Application: Optical Interconnect

Optical interconnect can be applied in all level of short range interconnects:

- Inside the box: intra-chip, intra-module (e.g. in Multichip Module (MCM)), intra-card, and card-to-card (motherboard) level
- Box-to-box level

It is a promising potential to solve performance problem, such as that faced by the Front Side Bus in a typical PC. Figure 6.1 shows the typical computer architecture of an Intel processor and chipset (consisting of the memory controller hub (MCH) and I/O controller hub (ICH) [5]. MCH connects the processor with high speed device, especially the main memory and graphic controller, while the ICH provides connection to lower speed peripheral buses, such as Ethernet, USB and audio devices.

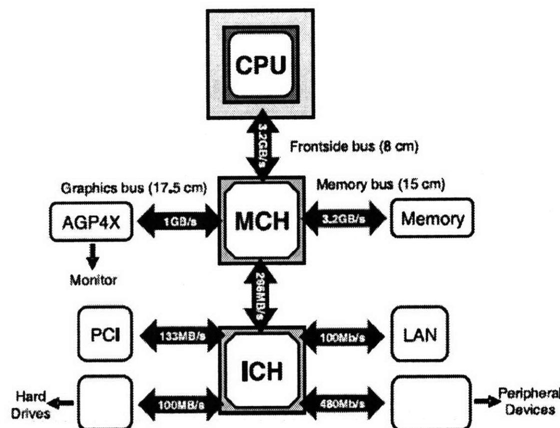

Figure 6.1: System architecture of a desktop PC [5]

The microprocessor clock speed has increased exponentially throughout the past few decades following the Moore's law. However, this increase is not scaling up with the increasing the front side bus (FSB) speed which connects the processor and the main

memory, as seen in Figure 6.2. This limits the system performance, as the processor will have to interrupt execution to wait for needed data to be fetched from memory. Similar problems exist in multiple processor system that shares an FSB.

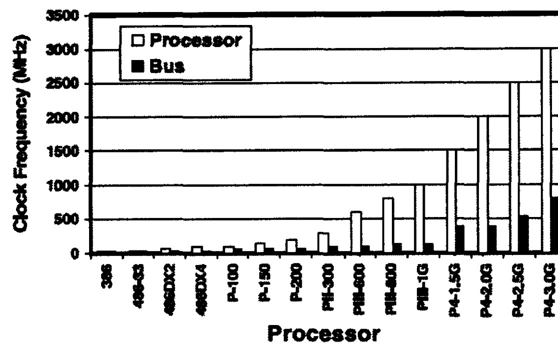

Figure 6.2: Frequency gap between the microprocessor and FSB over the last 15 years [5]

Several methods have been attempted to overcome this problem. One is by placing cache memory directly on the microprocessor so that it doesn't have to completely wait for the data from FSB. Architectural change by employing point-to-point architecture is another alternative. But eventually optical interconnect will still be an efficient solution, provided the cost of fabrication can be brought down to compete with the electronics counterpart.

The use of fiber, however, is not suitable in all level of interconnects mentioned above due to the relative size of the fiber as compared to other on-chip components. Thus optical solder is most likely to be applied in box-to-box level interconnect, and temporarily for board level interconnect.

Solution to the on-chip/board interconnect would be using waveguide instead of fiber. An example is the work by Ishii [26], where the waveguide was embedded in the motherboard PCB while a BGA package with VCSEL light source mounted on sits on top. The waveguide forms 45° TIR mirror at the end, which directs the light coming from VCSEL vertically to the horizontal waveguide.

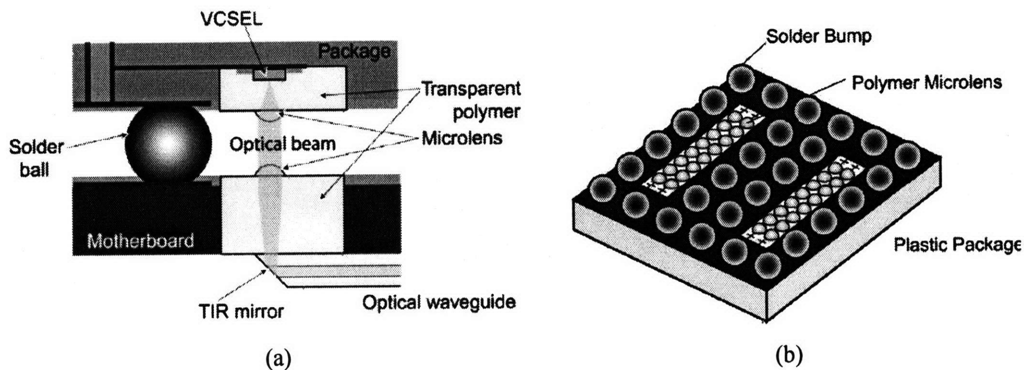

Figure 6.3: (a) Mechanism of light coupling through microlenses interface, (b) Schematic view of the solder bumps and microlenses arrays [26]

This structure, however, might not be the best solution for the light coupling due to its sensitivity to many fabrication variables, such as lens radius, alignment, etc. Another variation of this method is to use fiber underlying the chip, and to insert an optically transparent material in between the chip and PCB, a method patented by Lu [27], shown in Figure 6.4. The optically transparent material can either be acrylic or silicone-base. This method is more reliable as the optical path is now fully covered, but it can contain much less optical/electrical connection as most space is now taken by the fiber.

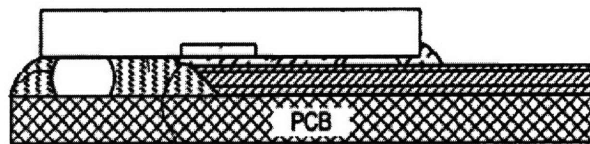

Figure 6.4: Underfilling chip/PCB space

The configuration proposed next is by using edge emitting laser, connecting the fiber by butt-coupling with the waveguide [28] as shown in Figure 6.5.

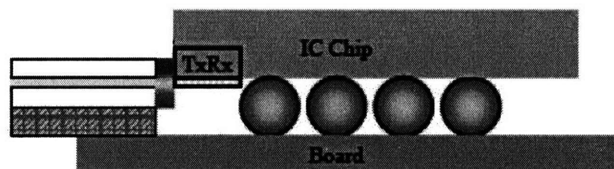

Figure 6.5: Fiber to waveguide butt coupling

The electrical connections are formed by the solder bumps spread through the area of the chip, while the optical connections are made by butt-coupling the fiber to the edge of the chip. High interconnect density can be achieved using this method.

6.2 The Package

6.2.1 Ball grid array (BGA)

There have been several evolutions to the packaging of electronic components. BGA is the most suitable packaging technique if the photonic components were to be integrated, as the optical connections can be built in the periphery of the chip without occupying the spaces for the electrical connections below. Besides, BGA is the lowest cost electrical chip mounting process available so far.

BGA provides some other advantages, such as shorter connection distance to the board resulting in faster speed and smaller footprint. The only disadvantage of this technology is the different thermal coefficient of expansion between the chip, solder, and substrate materials which can cause cracking and failure. This is overcome by underfilling the space in between the solder bumps by epoxy, thus will distribute the stress evenly at larger area.

6.2.2 Substrate modification

For the substrate, standard multilayer FR-4 printed circuit boards are analyzed, although other substrates can be easily integrated (e.g. in silicon substrates, grooves can be easily and accurate formed by etching processes). Grooves can be created on the FR-4 by fine-tip diamond saw, with liquid to flush the debris away during the fabrication. The fiber can be placed in the groove, leaving only longitudinal uncertainty during the fiber placement.

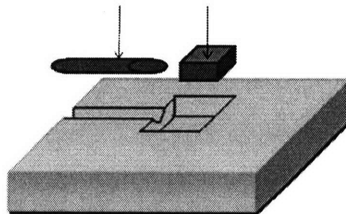

Figure 6.6: Substrate modification to make groove and hole for the fiber and chip to sit on

Flip-chip die (e.g. laser, PD) with the waveguide facing the PCB is placed side by side to the fiber. As the solder bump thickness is thicker than the cladding of the fiber (which cause vertical misalignment between the fiber and waveguide), some depression with the thickness incorporating the height offset of fiber/waveguide is created on the PCB.

6.2.3 Flip Chip Processes

As the name implies, chips are connected to the PCB by flipping the active area, such that it is placed face to face to the PCB, the connections are done by the solder bumps discussed above. The main processes in flip chip mounting are to place the bumped chip on the solder pad in the substrate, to reflow the solder in oven, to fill the chip/substrate gap with adhesive, and to cure the adhesive. All these can be done in several ways, depicted in Figure 6.7.

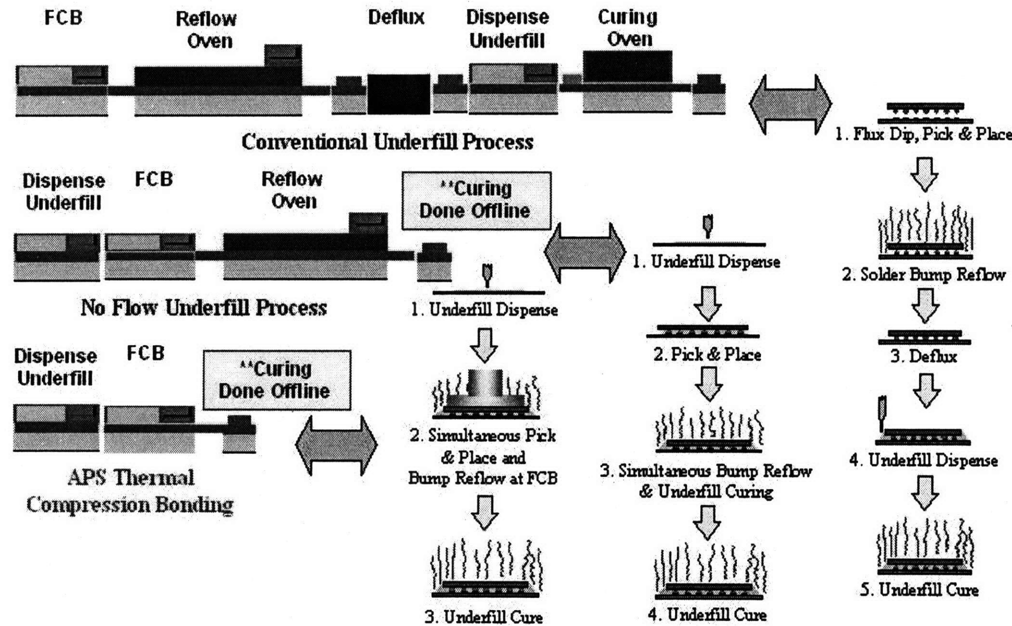

Figure 6.7: Various flip chip processes [29]

Best implementation of optical solder would be that with the least extra steps as compared to the existing flip chip processes. Two methods are proposed below.

Proposal 1: Incorporation with solder reflow processes

The optical solder is applied at the end of the fiber, either through coating or dipping process. It is then placed in the modified PCB using pick and place machine. In the next step, the bumped chip is placed in the designated hole with solder pads ready on the substrate. All these are brought in the solder reflow oven. The optical solder will flow and wet the waveguide. Both the optical and electrical connections are thus formed after the reflow process is done.

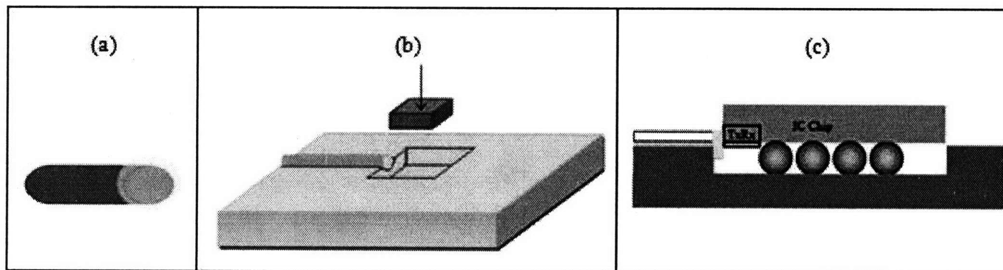

Figure 6.8: (a) Optical solder coated fiber, (b) Chip placement into the hole with optical solder coated fiber in place, (c) side view of the fiber and chip in place

To use this method, one must ensure the optical solder material to have low enough viscosity to flow and wet the waveguide, and high enough viscosity not to allow the optical solder to just drop down to the hole instead of sticking to the waveguide and stay there. The wetting property of the optical solder is thus very important as well.

Proposal 2: Incorporation with underfilling processes

A standard fiber is located on the groove together with the bumped chip using the pick and place machine. After the reflow process, an underfill is dispensed to fill the gap between the chip and substrate. Not only does this optical solder fill the underlying gap, it should be dispensed until the solder covers the optical path between the fiber and waveguide. This underfill material must thus be transparent and have low modulus of elasticity to bear the load generated due to thermal coefficient difference between the chip and substrate.

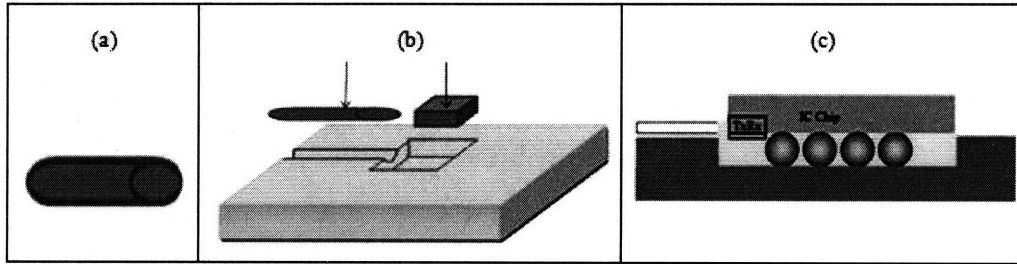

Figure 6.9: (a) Optical fiber, (b) Placement of fiber and chip on the groove and hole, (c) side view of the filled gap

The proposed methods, however, still contain various weaknesses, such as the materials selections, viscosity, etc. Further improvement needs to be done to obtain the optical solder best implementation methods.

6.3 Materials for Optical Solder

Based on the previous discussions, there are several important requirements an optical solder must have:

1. *Transparency at 1550nm*

   Light loss in polymer can be due to [30]:

   - Intrinsic factors – this determine the lower limit of loss in the polymer:
     a. Absorption:
        i. electronic transition absorption loss
        ii. harmonic of molecular vibrations: caused by the vth higher harmonic (overtone) v_v of the fundamental stretching vibration v_l and its combination tone $v_v+\delta$ with bending vibration δ
     b. Scattering: Rayleigh scattering loss caused by fluctuation of the density and refractive index in a polymer.
   - Extrinsic loss:
     a. Absorption: transition metals, organic contaminants
     b. Scattering: due to dust and microvoids, orientational birefringence, fluctuation in core diameter, core-cladding boundary imperfections, etc

The required wavelength for communication now is in the near-infrared regime. Of the loss mechanisms, Infrared energies are insufficient to induce electronic transitions but are able to excite vibration motions of molecules and parts thereof in condensed matter. The absorption mechanisms in near infrared wavelength are thus dominated by the overtone and combination bands of fundamental groups containing C-H, O-H, and N-H bonds. The table below summarizes the absorption bands common to organic molecules in the near infrared region.

Wavelength (nm)	Assignment
2200–2450	Combination C–H stretching
2000–2200	Combination N–H stretching, combination O–H stretching
1650–1800	First overtone C–H stretching
1400–1500	First overtone N–H stretching, first overtone O–H stretching
1300–1420	Combination C–H stretching
1100–1225	Second overtone C–H stretching
950–1100	Second overtone N–H stretching, second overtone O–H stretching
850–950	Third overtone C–H stretching
775–850	Third overtone N–H stretching

Table 6.1: Mechanism of absorption at various wavelengths [30]

It can be thus be inferred that all polymers will have some infrared-wavelength absorption due to the C-H and O-H bonds.

Attempt to reduce the absorption due to the overtone is to use deuterated (hydrogen with mass number 2) or halogenated polymers to replace most of the C-H bonds that causes absorption. But polymers made by deuterated polymers are rather expensive and it is not possible to reduce their cost. Many thus develop low loss polymer using the later, halogenated polymers.

2. *Refractive index matching that of fiber ~1.5*

   Previous results show that optical solder is insensitive to the refractive index variations. However, to reduce the external scattering loss due to fiber surface roughness when light comes out from the fiber, an index-matched optical solder should be used. The refractive index of polymers can be controlled by addition of

additives and/or proportioning the ratio of one polymer with the other(s) in a polymer mixture.

3. *Low glass transition temperature*

This requirement emerges from the fabrication processes. The glass transition temperature of the polymer must be low enough such that it can be processed with the solder bumping at the same time (maximum temperature ~210°C, Figure 6.10), i.e. to provide both the electrical and optical connections at the same time, and so that it won't spoil the other components which have low damage resistance to heat. It should also be high enough so the optical solder would have good load resistance at the service temperature.

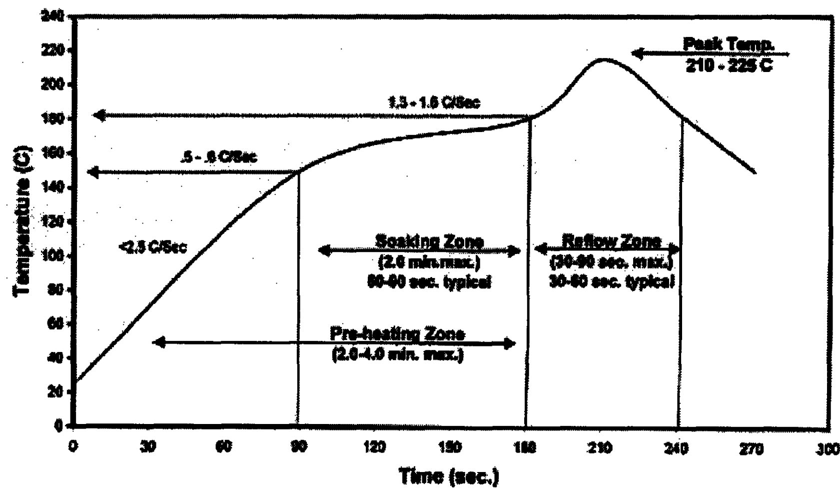

Figure 6.10: Typical solder reflow profile [31]

For process design that requires the materials to flow, thermoplastics should be used. Typical reflow process lasts for about 5mins, at maximum temperature of 210°C (Figure 6.10). Thus, the optical solder must have glass transition temperature below that temperature.

4. *Appropriate Temperature-Viscosity Profile*

Similar to point (3), we want the viscosity of the polymer to be just right when the maximum temperature in the solder reflow chamber is reached.

5. *Appropriate Solidification Rate*, to ensure that the solder is sufficiently hardened at the end of the solder reflow process.

6. *No Swelling or absorbance to contaminants*, otherwise it will degrade the light coupling capability.

Materials possible for optical solder application and their properties are listed in Table 6.2. They are materials used for optoelectronics for the last few decades and are qualified based on their optical properties.

Materials	Loss @ 1.55 µm (dB/cm)	T_g* (°C)	n	Trade product (Manufacturer)
Fluorinated polyimide		250-410	1.534 – 1.54	(NTT)
	0.6 [32]			Ultradel™ (Amoco)
Acrylate	0.5	25		(AlliedSignal)
	0.6		1.28-1.72 [33]	Polyguide™ (DuPont)
Fluorinated acrylate	0.07	-50	1.444 [34]	(AlliedSignal)
	1.7	110		(NTT)
Polycarbonate [35]	1.4 [36]	190	1.546 (TE), 1.543 (TM)	
Fluorinated copoly(arylene ether sulfide) [37]	0.2 – 0.5	> 300	1.51-1.60	
Benzocyclobutene	1.5	>350	1.541	Cyclotene™ (Dow Chemical)
Perfluorocyclobutane	0.25	400	1.4878	XU 35121 (Dow Chemical)

* T_g = glass transition temperature

' T_d = decomposition temperature

'' n = refractive index

Table 6.2: Potential materials for optical solder

Polymers with simple structure, such as polyolefins, syndiotactic polyvinyl chloride, etc, are not considered here as they can crystallize easily, resulting in reflections and low light transparency. Thermoset, e.g. epoxies, UV-cured polymers, are strong, but they are in

liquid form before curing and it normally takes complex and long curing time (> 30mins) at very high temperature, which is not compatible with the solder reflow process. Thermoplastic is the most appropriate material for this application, as it can flow when temperature increases beyond its T_g, and solidify again below T_g. Its reliability, however, needs to be addressed carefully as thermoplastic materials are more sensitive to environmental changes.

There are pros and cons for each material for its application as optical solder. Polycarbonate, for e.g. has appropriate T_g and refractive index, but the loss is quite high, compared to other polymers. Fluorinated polyimide has relatively low loss, with slightly higher T_g than the solder reflow temperature. It is still possible to use this material, probably by adjusting the solder reflow temperature profile. Nevertheless, these discussions are only based on the first three criteria: loss, refractive index and T_g. More works need to be done in the materials aspect.

6.4 Cost Analysis

Chip packaging costs 60-80% of the total IC cost, as shown in Figure 6.11. It includes the tool and cycle time required for the placing and alignments of the optical components. By using optical solder, the alignment tolerance is relaxed and thus the required equipment will be cheaper. For comparison, pick & place machines with accuracies around 3μm are five times lower than machines with < 1μm accuracy. Besides, the cycle time is much shortened as the passive alignment can be utilized with less compromise to the performance.

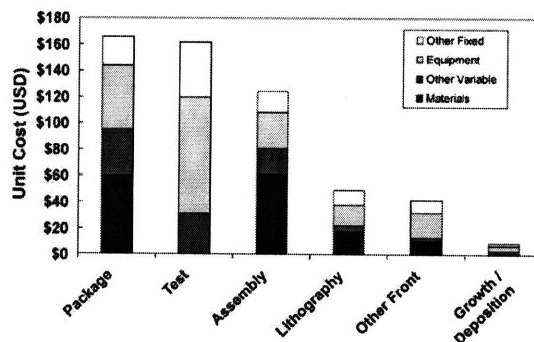

Figure 6.11: Typical cost induced in making an integrated circuit [38]

The materials, on the other hand, contribute to ~35% to the final package cost. Assuming 3μm gap between the fiber and waveguide, and the optical solder with diameter 125μm fills the gap, the volume of optical solder required per optical pin is ~61.36mm^3. If the optical solder costs tens of dollars per liter, the cost of optical solder per optical pin is only less than a cent. A single fiber cost around 4.75 cents per optical pin [28]. This shows that optical solder is a very cheap solution to the fiber-waveguide coupling problem.

Chapter 7 Conclusion

Optical solder has been studied in this thesis for application in fiber to waveguide light coupling as a potential solution to the coupling problem in optical interconnects. It is a simple coupling concept and has many advantages. Together with the inverse taper feature, it gives much higher coupling efficiency and thus misalignment tolerances. This allows lower power consumption, as the transmitter can now produce lower power signal – they will still be received with low BER at the receiver side. Besides, it is more reliable as the fiber is permanently joined to the waveguide; no external impurities can interfere which cause unnecessary scattering that degrades the optical signal. It can be cheaply integrated: there is also no fundamental fabrication issue, as it can be easily incorporated with the existing electronic processes with minimal tools modification, and the material cost is negligible. In conclusion, optical solder capability would be the revolutionary enabler for widespread use of electronic-photonic ICs.

Future work should concentrate on the materials aspect of the optical solder, and on how to achieve an increased coupling efficiency. Experimental data should also be obtained to compare with the theoretical results.

References

1. Sparacin, D.K., *Process and Design Techniques for Low Loss Integrated Silicon Photonics*, in *Material Science and Engineering.* 2006, MIT: Boston.
2. Huang, W.-P., *Optical Transceivers for FTTP Applications: System Requirements and Enabling Technologies.* J. Lightwave Tech., 2006. **25**: p. 11 - 27.
3. Mohammed, E., et al., *Optical Interconnect System Integration for Ultra-Short-Reach Applications.* Intel Technology Journal, 2004. **8**(2): p. 115-125.
4. Kimerling, L.C., et al., *Monolithic Silicon Microphotonics*, in *Silicon Photonics.* 2004, Springer Berlin.
5. Paniccia, M., M. Morse, and M. Salib, *Integrated Photonics*, in *Silicon Photonics.* 2004, Springer: Berlin. p. 1999.
6. Day, I., et al., *Tapered Silicon Waveguides for Low Insertion Loss Highly Efficient High-Speed Electronic Variable Attenuators.* Proc. IEEE OPt. Fiber COmmn. Conf., 2003. **1**: p. 23-27.
7. Doylend, J.K. and A.P. Knights, *Design and Simulation of an Integrated Fiber-to-Chip Coupler for Silicon-on-Insulator Waveguides.* Selected Topics in Quantum Electronics, IEEE Journal of, 2006. **12**(6): p. 1363-1370.
8. Masanovic, G.Z., V.M.N. Passaro, and G.T. Reed, *Coupling to nanophotonic waveguides using a dual grating-assisted directional coupler.* Optoelectronics, IEE Proceedings -, 2005. **152**(1): p. 41-48.
9. Nguyen, V., et al. *Asymmetric GRIN Lensed Single Mode Fiber-to-Waveguide Coupler.* in *Group IV Photonics, 2006. 3rd IEEE International Conference on.* 2006.
10. Nguyen, V., et al., *Silicon-based highly-efficient fiber-to-waveguide coupling for high index contrast systems.* Appl. Phys. Lett., 2006. **88**: p. 081112.
11. Lu, Z. and D. Prather, *Total Internal Reflection-Evanescent Coupler for FIber-to-Waveguide Integration of planar Optoelectric Devices.* Optics Letters, 2004. **29**(15): p. 7374-7378.
12. Laurent, V., et al., *Design, Realization, and Characterization of 3-D Taper for Fiber/Micro-Waveguide Coupling.* Selected Topics in Quantum Electronics, IEEE Journal of, 2006. **12**(6): p. 1354-1358.
13. Lee, K.K., et al., *Mode Transformer for Miniaturized Optical Circuits.* Optics Letters, 2005. **30**(5): p. 498-500.
14. Almeida, V.R., R.R. Panepucci, and M. Lipson, *Nanotaper for compact mode conversion.* Optics Letters, 2003. **28**(15): p. 1302-1305.
15. Johnson, S.G. and J.D. Joannopoulos, *Photonic Crystals: The Road from Theory to Practice.* 2002: Kluwer Academic Publishers.

16. Saleh, B.E.A. and M.C. Teich, *Fundamendals of Photonics*, ed. J.W. Goodman. 2001: John Wiley & Sons, Inc.
17. 2006 [cited 30 Juy 2008]; Available from: http://cache.eb.com/eb/image?id=96591&rendTypeld=4.
18. Drakos, N. *Propagation in Optical Fibers*. 1996 [cited 30 July 2008].
19. *Polarization*. 2008 [cited 30 July 2008]; Available from: http://en.wikipedia.org/wiki/Polarization.
20. Manolatou, C., *Passive Components for Dense Optical Integration Based on High Index-Contrast*, in *Department of Electrical Engineering and Computer Science*. 2001, Massachusetts Institute of Technology: Cambridge. p. 185.
21. Farjadpour, A., et al., *Improving Accuracy by Subpixel Smoothing in the Finite-Difference Time Domain.* Optics Letters, 2006. **31**(20): p. 2972-2974.
22. *Finite-Difference Time-Domain Method.* 2007 [cited 2008 15 July 2008]; Available from: http://en.wikipedia.org/w/index.php?title=Finite-difference_time-domain_method&oldid=120293931
23. Yee, K., *Numerical solution of inital boundary value problems involving maxwellapos;s equations in isotropic media.* Antennas and Propagation, IEEE Transactions, 1966. **14**: p. 302-306.
24. Taflove, A., *Computational Electrodynamics: The Finite-Difference Time-Domain Method.* 1995, Norwood, MA: Artech House, Inc.
25. Montalbo, T.M., *Fiber to Waveguide Couplers for Silicon Photonics*, in *Department of Materials Science and Engineering*. 2004, Massachusetts Institute of Technology: Cambridge.
26. Ishii, Y., et al., *Fully SMT-Compatible Optical-I/O Package with Microlens Array Interface.* J. Lightwave Tech., 2003. **21**(1).
27. Lu, D., *Underfill Integration for Optical Packages*. 2007, Intel Corporation.
28. Lee, C.-f., *Packaging Solution for VLSI Electronic Photonic Chips*, in *Materials Science and Engineering*. 2007, Massachusetts Institute of Technology: Cambridge. p. 44.
29. *Process for Flip Chip on Substrate.* [cited 10 August 2008]; Available from: http://www.advanpack.com/latestEvent.html.
30. Takezawa, Y., et al., *Empirical estimation method of intrinsic loss spectra in transparent amorphous polymers for plastic optical fibers.* Journal of Applied Polymer Science, 1992. **46**(10): p. 1835 -1041.
31. *Maxim Wafer-Level Package Assembly Guide.* [cited 10 August 2008]; Available from: http://www.maxim-ic.com/appnotes.cfm/an_pk/3377.
32. Kobayashi, J., et al., *Fluorinated polyimide waveguides with low polarization-dependent loss and their applications to thermooptic switches.* Lightwave Technology, Journal of, 1998. **16**(6): p. 1024-1029.

33. Eldada, L., *Organics in Optoelectronics: Advances and Roadmap*. 2005, DuPong Photonics Technologies: Wilmington, MA.
34. Kim, K.R., K. Oh, and C. Selee. *Refractive microlens on fiber using UV-curable fluorinated acrylate polymer by surface-tension induced self-assembly*. in *Lasers and Electro-Optics, 2003. CLEO '03. Conference on*. 2003.
35. Kang, J.-W., et al., *Low Loss Polymer Optical Waveguides with High Thermal Stability*, in *Materials Research Society Symposium Proceeding*. 2002.
36. Kang, J.-W., J.-S. Kim, and J.-J. Kim, *Optimized Oxygen Plasma Etching of Polycarbonate for Low-Loss Optical Waveguide Fabrication*. J. Appl. Phys., 2001. **40**: p. 3215-3219.
37. Jae-Wook, K., et al., *Structure-property relationship of fluorinated co-poly(arylene ether sulfide)s and co-poly(arylene ether sulfone)s for low-loss and low-birefringence waveguide devices*. Lightwave Technology, Journal of, 2005. **23**(1): p. 364-373.
38. Fuchs, E.R.H., et al., *Process-based cost modeling of photonics manufacture: the cost competitiveness of monolithic integration of a 1550-nm DFB laser and an electroabsorptive modulator on an InP platform*. Lightwave Technology, Journal of, 2006. **24**(8): p. 3175-3186.